JOURNAL OF GEOPHYSICAL RESEARCH, VOL. 104, NO. B9, PAGES 20,133–20,151, SEPTEMBER 10, 1999

Premonitory slip and tidal triggering of earthquakes

David A. Lockner and Nick M. Beeler

US Geological Survey, Menlo Park, California

Abstract. We have conducted a series of laboratory simulations of earthquakes using granite cylinders containing precut bare fault surfaces at 50 MPa confining pressure. Axial shortening rates between 10^{-4} and 10^{-6} mm/s were imposed to simulate tectonic loading. Average loading rate was then modulated by the addition of a small-amplitude sine wave to simulate periodic loading due to Earth tides or other sources. The period of the modulating signal ranged from 10 to 10,000 s. For each combination of amplitude and period of the modulating signal, multiple stick-slip events were recorded to determine the degree of correlation between the timing of simulated earthquakes and the imposed periodic loading function. Over the range of parameters studied, the degree of correlation of earthquakes was most sensitive to the amplitude of the periodic loading, with weaker dependence on the period of oscillations and the average loading rate. Accelerating premonitory slip was observed in these experiments and is a controlling factor in determining the conditions under which correlated events occur. In fact, some form of delayed failure is necessary to produce the observed correlations between simulated earthquake timing and characteristics of the periodic loading function. The transition from strongly correlated to weakly correlated model earthquake populations occurred when the amplitude of the periodic loading was approximately 0.05 to 0.1 MPa shear stress (0.03 to 0.06 MPa Coulomb failure function). Lower-amplitude oscillations produced progressively lower correlation levels. Correlations between static stress increases and earthquake aftershocks are found to degrade at similar stress levels. Typical stress variations due to Earth tides are only 0.001 to 0.004 MPa, so that the lack of correlation between Earth tides and earthquakes is also consistent with our findings. A simple extrapolation of our results suggests that approximately 1% of midcrustal earthquakes should be correlated with Earth tides. Triggered seismicity has been reported resulting from the passage of surface waves excited by the Landers earthquake. These transient waves had measured amplitudes in excess of 0.1 MPa at frequencies of 0.05 to 0.2 Hz in regions of notable seismicity increase. Similar stress oscillations in our laboratory experiments produced strongly correlated stick-slip events. We suggest that seemingly inconsistent natural observations of triggered seismicity and absence of tidal triggering indicate that failure is amplitude and frequency dependent. This is the expected result if, as in our laboratory experiments, the rheology of the Earth's crust permits delayed failure.

1. Introduction

Tidal forces exerted by the Moon and Sun produce continuously varying stresses throughout the Earth's crust of the order of 0.001 to 0.004 MPa [*Melchior,* 1983; *Vidale et al.,* 1998b]. Given the slow accumulation of stress along active faults due to plate motion and other tectonic processes, it has long been postulated that the fluctuations in stress due to Earth tides might be sufficient to trigger earthquakes [*Cotton,* 1922; *Klein,* 1976; *Heaton,* 1982]. With few exceptions, careful analyses of quality data sets suggest that little or no correlation exists between Earth tides and earthquakes [*Heaton,* 1982; *Rydelek et al.,* 1988; *Hartzell and Heaton,* 1989; *Rydelek et al.,* 1992; *Tsuruoka et al.,* 1995; *Vidale et al.,* 1998b]. Most recently, *Vidale et al.* [1998b] have carried out tensor analysis on a set of 13,042 earthquakes occurring on the San Andreas and Calaveras faults in California and have found no statistically significant correlation between earthquake occurrence and either tidal stress or stressing rate. One possible exception is a study of 35 moderate to large southern California earthquakes by *Kilston and Knopoff* [1983]. They found no correlation between the timing of smaller events ($5.9 \geq M \geq 5.3$) and periodicity of solar or lunar tides. However, the 13 largest earthquakes ($M \geq 6$) showed statistically significant correlations with sunrise/sunset and new/full Moon. Curiously, they found no correlation with moonrise/moonset which, because of the stronger tidal influence of the Moon, would be expected to show a stronger correlation than that of sunrise/sunset. A sampling of only 13 earthquakes is small for a statistical study of this kind and the significance of this result remains uncertain.

The general lack of correlation between earthquakes and Earth tides becomes even more interesting when compared with seismicity on the Moon. Natural lunar seismicity is essentially of two types: random impact of meteoroids and repeating deep-focus earthquakes occurring in two bands at depths of 800 to 1000 km [*Lammlein et al.,* 1974]. Peak moonquake activity occurs at 13- to 14-day intervals and is clearly associated with the variation in lunar tidal forces with a fortnightly period of ~13.7 days. Because of its greater mass, the Earth exerts a significantly larger tidal stress on the Moon than the Moon exerts on the Earth. However, the Moon's

Paper number 1999JB900205.

rotation is synchronized with its orbit and the tidal influence of the Earth is essentially static. The dominant time-varying tidal stress on the Moon results from the gravitational pull of the Sun and is significantly smaller than the tides on the Earth [*Melchior,* 1983]. Even so, lunar tides have a dominant role in the timing of moonquakes. It has also been suggested that the lack of water on the Moon may affect the sensitivity of moonquakes to stress variations. However, it is not clear how the amount of free water at the surface affects the water content at 800 km depth. We do not attempt to explain the strong correlation of lunar tides and moonquakes in the present paper. It is, however, an observation that must eventually be reconciled with any comprehensive model of tidal triggering.

We suggest that the question of earthquake triggering should be examined both in terms of the amplitude and frequency of the forcing function which is expected to induce failure. We will present laboratory evidence showing that for large amplitude stress increases, the earthquake response can be considered essentially instantaneous. However, for modest stress increases a nucleation phase involving premonitory, accelerating slip leads to a time delay between the imposed stress change and the resulting earthquake [*Johnson,* 1981]. Thus, to properly model the interaction of the subtle, time-dependent stress changes occurring in the Earth's crust and the timing of earthquakes, it is essential that time-dependent rheology or some process involving delayed failure be included in the analysis. *Dieterich* [1987] reached a similar conclusion following theoretical analysis of a class of laboratory derived fault friction rheologies generally referred to as rate- and state-dependent friction equations. These constitutive equations lead to an accelerating fault nucleation phase that provides an inherent time delay between the application of a stress or displacement perturbation and the resulting fault instability. Dieterich's model makes a number of specific testable predictions, some of which we will evaluate in this study.

With the continual improvement of seismological and other geophysical monitoring equipment, additional observations are being made that relate to the question of stress triggering of earthquakes. Static stress changes have now been calculated for a number of moderate earthquakes in an attempt to relate the spatial distribution of aftershocks to regions of inferred stress increase [*Reasenberg and Simpson,* 1992; *King et al.,* 1994; *Stein et al.,* 1994; *Harris et al.,* 1995]. While positive correlations have been reported for increases in the Coulomb failure function (CFF) of 0.1 MPa or more, calculated stress increases of less than 0.01 to 0.05 MPa generally show no correlation with increased seismicity [*Hardebeck et al.,* 1998]. Furthermore, the time-dependent nature of aftershock sequences is such an ubiquitous and fundamental phenomenon that it is referred to as Omori's aftershock decay law. This delay between stress change and aftershock response is probably the clearest evidence that earthquake triggering involves time-dependent processes.

Radiated seismic energy provides an additional test for the conditions under which earthquake triggering can occur. Stress fluctuations due especially to surface waves [*Hill et al.,* 1993; *Anderson et al.,* 1994; *Gomberg and Bodin,* 1994; *Gomberg and Davis,* 1996] are significantly larger than Earth tide stresses but also occur at much higher frequencies. Although there is evidence for remote triggering of earthquakes following the Landers earthquake, the reported increased seismicity was in selected areas commonly associated with magma intrusion [*Hill et al.,* 1993] or areas of preexisting high seismicity rates [*Anderson et al.,* 1994]. In any case, widespread and immediate triggering of earthquakes by dynamic waves is apparently uncommon. This does provide an important test, however, for any model that is developed to explain tidal triggering (or lack thereof). *Gomberg and Davis* [1996] noted a correlation between the passage of dynamic stress waves and increased seismicity at The Geysers, California. They concluded that a threshold of approximately 0.1 to 0.4 μstrain was needed to trigger seismicity in this region. Using a representative shear modulus of 30 GPa, this strain threshold is roughly equivalent to a shear stress threshold of 0.003 to 0.012 MPa. *Anderson et al.* [1994] concluded that a dynamic stress wave amplitude of 0.6 to 0.9 MPa was needed to trigger seismicity in the eastern California and Nevada region following the 1992 Landers earthquake.

Given the number of unsuccessful attempts to extract tidal correlations from earthquake catalogues, a different approach to explaining the sensitivity of earthquake failure to periodic stressing is warranted. We have chosen to generate model earthquake catalogues using laboratory-scale faults and "stick-slip" events which are the laboratory equivalent of earthquakes. By adding a small-amplitude sine wave to a constant loading rate, we have attempted to create a simplified model of the natural stressing conditions experienced by crustal faults. In this paper we report on the conditions under which correlations were observed between the periodic loading function and the occurrence of laboratory-scale earthquakes.

2. Experimental Procedure

The experiments reported in this paper provide laboratory-scale model earthquake catalogues under known and carefully controlled conditions of stress and displacement. Right cylinders of Westerly granite were prepared with diameters of 76.2 mm and nominal lengths of 190.5 mm. A saw cut inclined 30° to the sample axis was used as a sliding surface (Figure 1). Samples were deformed in a triaxial loading frame at constant confining pressure. In all experiments a constant axial shortening rate was imposed by a 1000 ton hydraulic ram using a fast acting servo designed to control the position of the loading piston at a point outside the pressure vessel. A 22-bit resolution displacement reference signal was updated 5 times per second, providing control resolution of 0.005 μm (or approximately 0.0003 MPa shear stress). This computer reference signal provided a ramp function V_r = 0.001, 0.01, or 0.1 μm/s axial shortening rate to mimic constant tectonic loading of the fault. Using an analog summing circuit, a second signal was then added to the constant loading rate input to impose periodic loading of the fault. This modulating signal was a sine wave provided by an HP3325A signal generator. Input amplitudes ranged from 20 to 200 mV, with a range in frequency of 10^{-4} to 10^{-1} Hz. For the particular input circuitry characteristics used, a 20-mV signal represents approximately 1.1-μm displacement (u_m) at the control point. Given the test machine stiffness and the fact that both shear and normal stress resolved on the fault surface change with axial load, a 20 mV signal results in approximately 0.07- and 0.04-MPa changes in shear and normal tractions resolved on the fault surface.

To insure stick-slip deformation rather than stable sliding, the sawcut surfaces were polished in the following manner: saw cuts were first surface ground to insure that they would be flat and well mated. They were then lapped against each other suc-

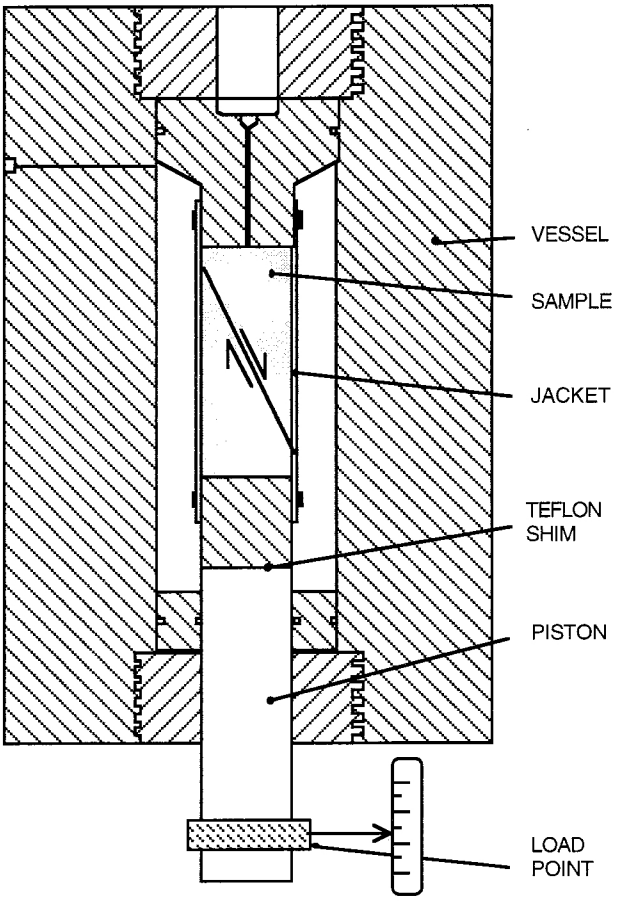

Figure 1. Triaxial test geometry for experiments showing granite sample with bare sawcut surface mounted in pressure vessel.

cessively with #120, 400, and 600 SiC abrasive. Following this fault surface polishing procedure, a sample was then jacketed in a polyurethane tube with adjoining steel end pieces and placed in the pressure vessel. A 0.13-mm-thick teflon shim was greased and placed between the steel end piece and loading piston to minimize resistance to lateral slip. After applying confining pressure, the sample was subjected to an initial run-in period of 1.5- to 2-mm axial shortening to allow shear strength to rise to a relatively constant level. At this point the desired loading rate and modulating signal were applied and axial displacement, confining pressure, and axial load were recorded. Given the limited total displacement available in this test geometry, we attempted to record approximately 20 stick-slip events at each set of test parameter values. We determined that this was a sufficient statistical sampling to identify conditions under which a strong correlation existed between the forcing function and the occurrence of stick-slip events. In this regard the present set of experiments should be considered a reconnaissance study, and more detailed delineation of weak interactions between the modulated input and resulting stick-slip events will require much larger statistical samples.

After 14 mm of axial shortening the confining pressure was removed so that the sample could jump back to its starting position because of elastic recovery of the polyurethane jacket. Then confining pressure was reapplied, and a second set of stick-slip events was recorded. At the high normal stress (roughly 80 MPa) used in these experiments, wear products consisting of a fine granite power developed on the fault surfaces during successive stick-slip events. As this fault gouge accumulated, the frictional properties of the sliding surfaces gradually changed until a transition from stick-slip to stable sliding occurred. We found that a sample could only be used for two passes before the transition to stable sliding occurred. At this point the sample was removed and the sawcut surfaces repolished as described above. This procedure resulted in good reproducibility of the sequence of stick-slip events spanning approximately 25 mm of total fault slip. Given the slow loading rates required for many of the test runs, the experiments reported here represent approximately 6 months of continuous machine time.

Resolution of axial displacement, at the control point outside the pressure vessel, was ±0.6 μm, although the control signal for the displacement ramp was about 100 times finer resolution. Confining pressure resolution and control were ±0.02 and ±0.1 MPa, respectively. Axial load was measured inside the pressure vessel with a resolution of ±0.05 MPa. While fault displacement was not measured directly, elastic loading of the sample column was well characterized (120 MPa/mm axial load) and could be removed from the axial displacement record to provide a calculated fault slip. Pressure, axial load, and displacement were recorded at a rate of one sample/s in the fast experiments and averaged to as much as 5-s intervals in the slowest experiments.

3. Experimental Results

3.1. Stick-Slip Sequences

A typical measurement sequence conducted at 50 MPa confining pressure is shown in Figure 2, in which differential stress is plotted as a function of axial shortening. A series of 49 stick-slip events were recorded in 13 mm axial displacement. After 2 mm displacement, peak stress remains nearly constant (coefficient of friction $\mu = \tau/\sigma_n \sim 0.68$), while the stress drop gradually increased with continued displacement. A stick-slip cycle occurring at 8 mm displacement is shown in greater detail in Figure 3. Average loading rate V_r was 0.01 μm/s, which produced stick-slip events at approximately 8-hour intervals. The sine wave modulation of the average loading rate had a period of 2326 s and amplitude of 50 mV on the control signal input. This periodic fluctuation resulted in the small-amplitude ripples in the stress and displacement records shown in Figure 3. In this case, shear stress oscillations were approximately ±0.12 MPa. The final 5000 s, representing about two cycles of the modulating signal, are shown in Figure 4. Important features to notice are the accelerating slip on the fault surface preceding failure by at least 400 s and the accompanying decrease in stress leading into the stick-slip event. Also plotted in Figure 4 is a quantity we refer to as the Coulomb failure function (ΔCFF) which is used to infer, for example, whether changes in regional stress resulting from an earthquake would accelerate or retard the failure of nearby faults [*Simpson and Reasenberg,* 1994; *Harris et al.,* 1995; *Stein et al.,* 1996]. In the absence of fluid pressure we can define ΔCFF as

$$\Delta CFF = (\tau - \tau_o) - \mu(\sigma_n - \sigma_{no}) \quad (1)$$

where τ_o and σ_{no} represent an arbitrary reference stress state.

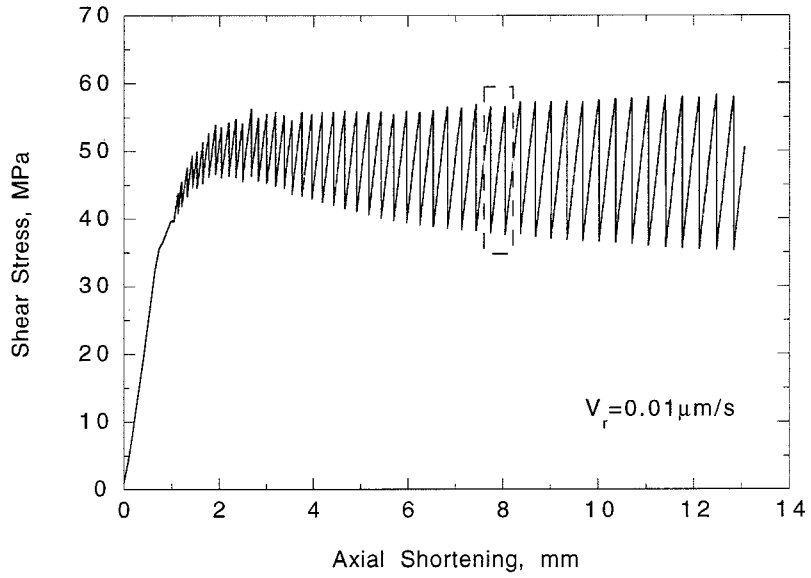

Figure 2. Differential stress versus axial displacement as measured at the control point outside the pressure vessel in a typical deformation sequence. Dynamic stress drops, referred to as stick-slip events, are the laboratory equivalent of earthquakes.

Equation (1) follows directly from the Coulomb failure criterion

$$\tau = C + \mu' \sigma_n, \tag{2}$$

where C is cohesion and μ' is one definition of coefficient of friction. (The standard operating definition of coefficient of friction that we use in this paper is $\mu = \tau/\sigma_n$. For $\tau >> C$, a condition appropriate for the experiments described here, μ and μ' are essentially equivalent.) By choosing τ_o and σ_{no} as stress values at the point of failure, then the simple Coulomb failure model requires that for $\Delta CFF < 0$ the fault will be stable and that failure occurs when $\Delta CFF = 0$. Included at the bottom of Figure 4 is a time plot of ΔCFF showing positive values for 700 s before failure a condition which, strictly speaking, violates the basic assumption of the Coulomb failure model. A maximum value of +0.2 MPa is reached about 5 min before failure, indicating that failure does not occur abruptly. Rather, failure involves a period of accelerating fault slip and fault weakening which becomes unstable when the weakening rate of the fault exceeds the elastic unloading rate of the driving system [*Ruina,* 1983; *Lockner and Byerlee,* 1990]. A variety of processes may be involved in earthquake nucleation. For the present discussion it is only important to recognize that a measurable delay occurs between the initiation of fault yielding and the time of unstable slip. This delay in the breakdown process is of fundamental importance in understanding the dependence of earthquake triggering on transient stressing sources such as tidal stressing and earthquake stress transfer. In rock mechanics, delayed failure is referred to as static fatigue and is a wellknown phenomenon [*Kranz,* 1980; *Lockner,* 1998]. For rupture of intact rock at constant load the time to failure is sensitive to stress level. For example, a decrease in applied load of only 0.2% in granite at 50 MPa confining pressure can delay failure by 25% [*Lockner,* 1998]. The variations in shear stress shown in Figure 4 are about 0.2% and by analogy can be expected to have a significant effect on advancing or delaying the time of failure. As we will show in section 3.2, this is, in fact, the case.

Given that our experiments were conducted at constant confining pressure and using faults inclined 30° to the sample axis, changes in shear and normal tractions on the fault surface were fixed in the ratio $\Delta\tau/\Delta\sigma_n = 1.732$. Then, for $\mu = 0.68$, Coulomb failure function and shear stress cannot vary independently: $\Delta CFF \cong 0.61\Delta\tau$. For the remainder of this paper we will report results primarily in terms of shear stress amplitude, although conversion to Coulomb failure function can be accomplished by reducing shear stress by 39%.

The stress oscillations shown in Figures 3 and 4 are of small enough amplitude that prior to the stick-slip nucleation phase, stress is monotonically increasing. An example more like tidal loading is shown in Figures 5 and 6. In this example the average loading rate was 0.001 μm/s with a modulating signal shear stress amplitude of 0.069 MPa and 50-s period. In this case, reversals in stress occurred regularly during the long term loading cycle (Figure 6). As in the preceding example, premonitory fault slip began at least 300 s before the stick-slip event and was accompanied by a gradual strength loss of about 0.1 MPa.

The complete set of measurements is summarized in Table 1. The timing of stick-slip events in these experiments is the result of a combination of stochastic and deterministic processes. Consequently, we will use statistical tests to determine the degree of correlation between the timing of stick-slip events and the oscillating loading function. While large numbers of events are desirable in demonstrating statistical significance, practical limitations required that the sample population for each combination of test parameters was limited to approximately 20 stick-slip events. This sampling number proved adequate to identify conditions for which strong correlations existed.

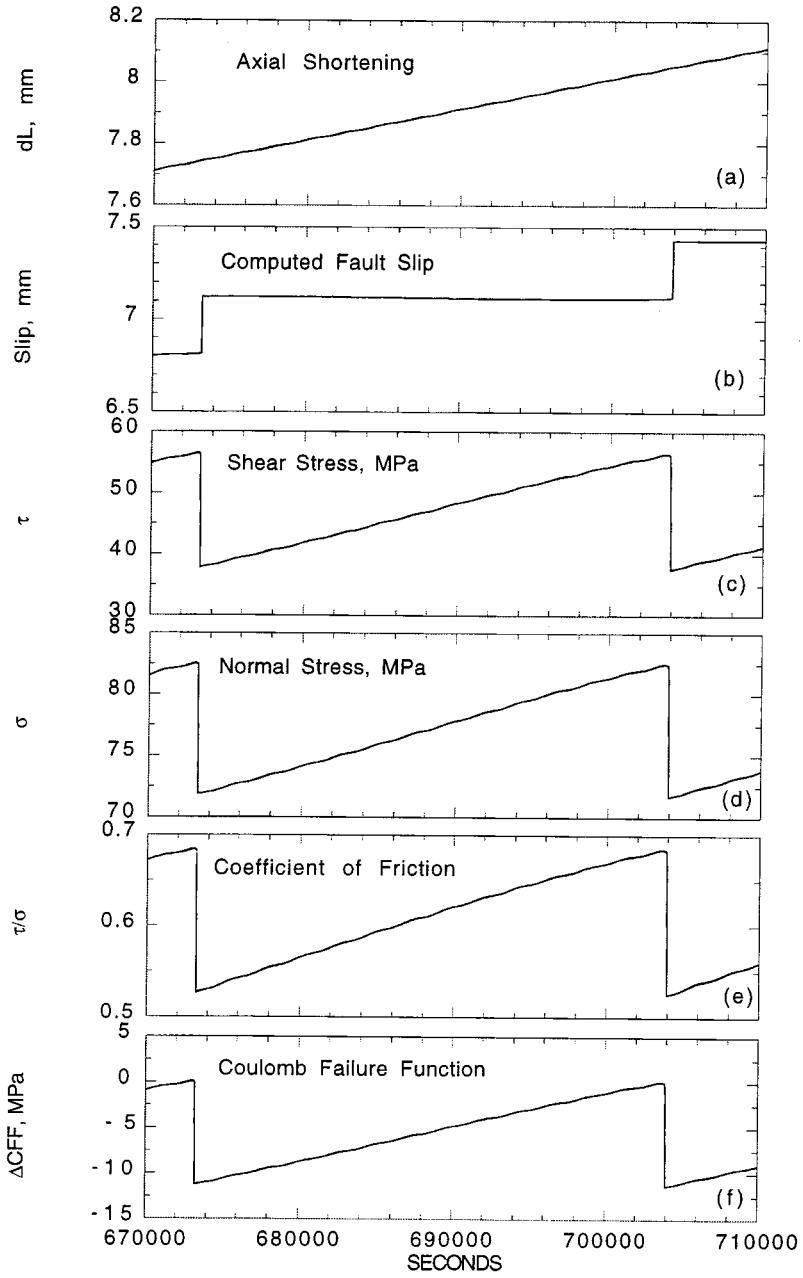

Figure 3. Time history of two stick-slip events indicated in Figure 2. Remote axial displacement was the control variable showing a steady loading rate superimposed with a small-amplitude sine wave (Figure 3a). Loading conditions were as follows: V_r = 0.01 μm/s and for the modulating signal, period equals 2326 s, and amplitude U_m = 1.3 μm (τ_m ~0.21 MPa). Computed fault slip (Figure 3b) shows that the fault was nearly locked over the entire loading cycle so that the stress changes were essentially an elastic response to the remote loading.

3.2. Schuster Test

We begin by asking if any sample sets allow us to reject the null hypothesis of random occurrence; that is, there is no correlation between the forcing function and the timing of stick-slip events. For a given sample set we simply note the angular phase θ of the occurrence of each stick-slip event relative to the forcing function. By convention, we use a cosine function so that a stick-slip event occurring at the peak in the displacement or stress occurs at $\theta = 0$. The phase shift between the peak seismicity rate and the peak amplitude of the forcing function will be denoted by ϕ. The sequence of stick-slip events can be treated as a random walk problem in which each event results in a unit length step in the direction defined by its phase angle. If the sequence of stick-slip events is random, it will wander, on average, a distance $D = \sqrt{N}$ from the origin, where N is the number of events. *Schuster* [1897] and *Rydelek and Hass* [1994] developed a simple expression for the probability P_{rw} that a random walk will end within a given distance D of the origin:

$$P_{rw} = \exp\left(-D^2/N\right) \tag{3}$$

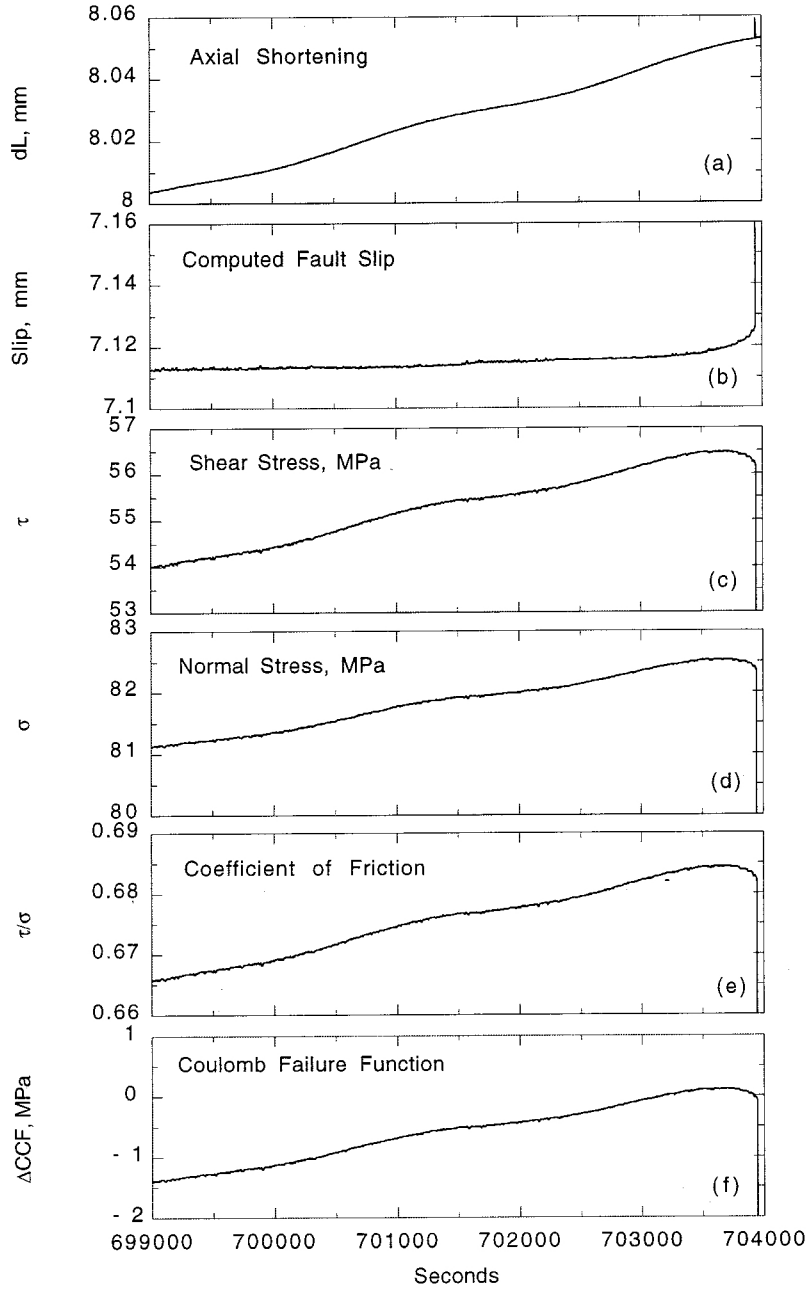

Figure 4. Final 5000 s history for the stick-slip event shown in Figure 3. At this magnification, premonitory creep and the accompanying fault weakening are clearly observable in the final 300 to 500 s. This delayed failure is important in determining how the stress oscillations will interact with stick-slip event timing.

A sample set containing a nonrandom component correlated with phase will produce a drift in the random walk away from the origin at a rate faster than $\sqrt{N}$. Pathological cases such as correlated events occurring at phases 180° apart and exactly canceling each other are possible but are unlikely in these tests. As an example, we plot three stick-slip sequences in Figure 7 using oscillating shear stress amplitudes τ_m of 0, 0.17 and 0.35 MPa. The 0.35 MPa sequence shows a steady drift with a phase angle of θ = -20°. The hypothesis that this sequence of events is random (uncorrelated with the forcing function) can be rejected at the 99.6% confidence level.

The zero-amplitude sequence was carried out to show that correlated events are, in fact, due to the periodic forcing function and are not the result of some unwanted periodic response that might be present in the loading system. Since each sequence of stick-slip events is run continuously without adjustment of the forcing function signal, the timing of the ith event can be expressed as $t_i = t_0 + T(m_i + \theta/(2\pi))$, where t_0 is the start of the sequence, T is the period of the forcing function, and m_i is the integer number of cycles that have elapsed before the ith event. When this formula is used to test for correlated events in the zero amplitude sequence, we find

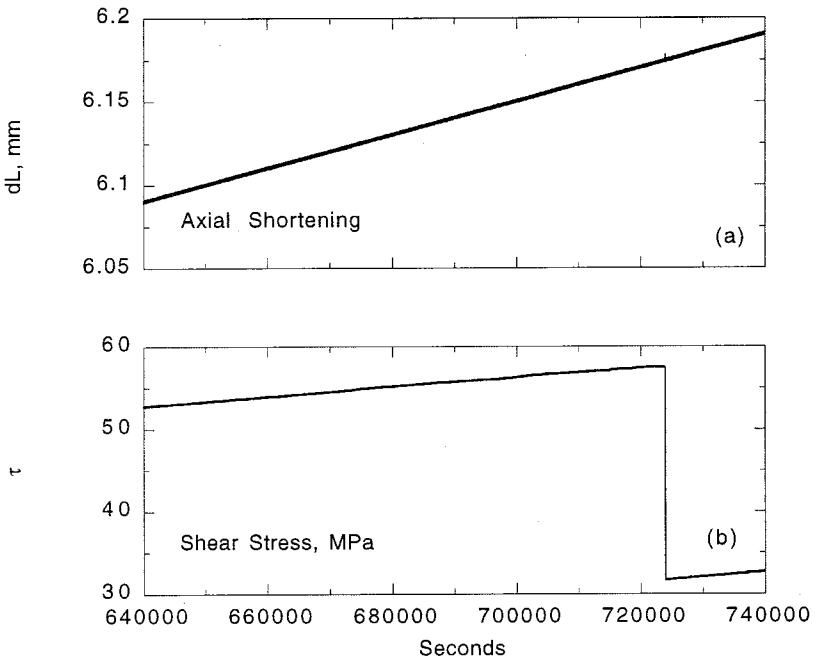

Figure 5. Second example of a stick-slip event under loading of V_r = 0.001 μm/s, modulating signal period equal to 50 s and amplitude U_m = 1.1 μm (~0.069 MPa). Thickness of displacement line is due to rapid oscillations.

that, indeed, event timing cannot be distinguished from random. Since the 0.35 MPa sequence shows a strong correlation, we expect that the 0.17 MPa test should at least contain a weak tendency for events to occur near θ = -20°. However, with a 23-event sampling, no statistically significant correlation has emerged. Apparently, a larger sampling is needed for a weak correlation to be observed (see the appendix). The quantity 1-P_{rw} is listed in Table 1 for all the test sequences. This parameter expresses the confidence with which the null hypothesis, that the sequence of stick-slip events occur at random phases, can be rejected. At all frequencies the largest amplitude tests showed strong correlation between stick-slip timing and the phase of the forcing function. In all cases we were able to reduce the amplitude of the forcing function until the occurrence of stick-slip events could no longer be distinguished from random.

In Figure 8 we have drawn the 95% confidence levels bounding the regions where a strong correlation exists between stick-slip event timing and the periodic forcing function. In general, larger-amplitude signals are better correlated that smaller-amplitude signals. Finer details of the 95% confidence contours, such as the presence of a minimum in each curve, are suggested but are not required by the present observations. Unambiguous determination of the detailed shape of these curves will require stick-slip sets that contain larger numbers and are more closely spaced in frequency and amplitude.

3.3. Two-Component Model

One property of the Schuster statistic described in section 3.2 is that the confidence levels, as plotted in Figure 8, should migrate to lower amplitude as the number of sampling events increases. This feature is discussed in the appendix. Basically, as the test population increases, a nonrandom component will cause the trajectories plotted in Figure 8 to drift farther and farther in a preferred direction. The probability that such a sequence can be explained by random chance becomes smaller and smaller, and the parameter 1-P_{rw} will increase with increasing N. To avoid this undesired effect, we present a different approach to analyzing the stick-slip event catalogues which gives a result that is stable with respect to the number of events sampled.

As with Earth tides, we restrict ourselves to oscillatory loading with a period shorter than the average repeat time of earthquakes on a given fault segment. We assume that for a periodic loading function with vanishingly small amplitude, the timing of stick-slip events should show no correlation to the period of the loading function. When a large number of earthquakes is considered, the expected seismicity should be independent of the phase of the loading function. As the amplitude of the forcing function increases, it should influence seismicity by either advancing or retarding the occurrence of individual events, depending on when they would have occurred during the loading cycle. We expect that increased stress or strain levels would promote earlier failure and decreased stress or strain would delay failure. As the amplitude of the forcing function increases, deviations from the average seismicity rate should also increase. By normalizing the expected seismicity rate, we obtain the probability density function, or PDF, of the seismicity with respect to the phase θ of the loading function. In the case of tidal triggering we anticipate that the small amplitude of the periodic loading function will produce correspondingly small deviations from the average seismicity rate.

On the basis of the preceding arguments we propose a simple model for seismicity rate composed of two additive terms: a purely random component and a periodic component with the same frequency as that of the forcing function. We

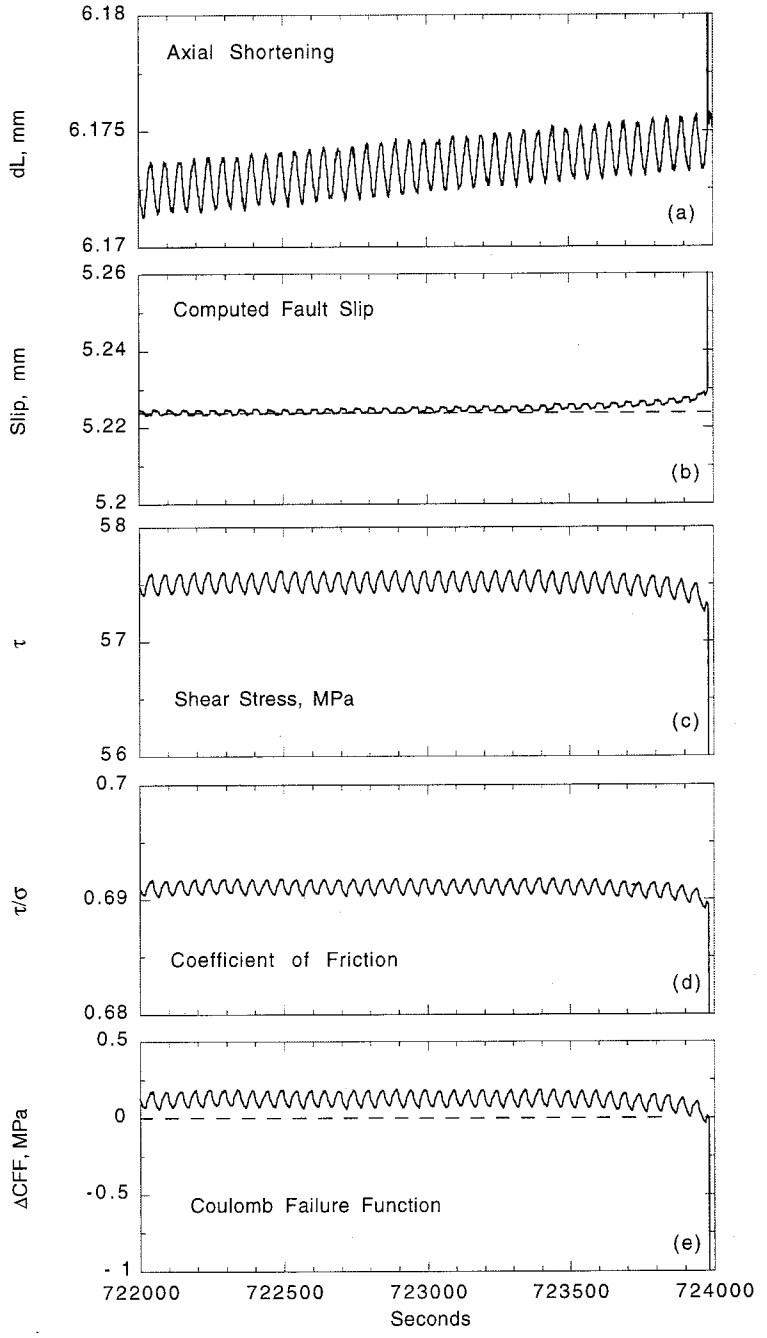

Figure 6. Final 2000 s history for the stick-slip event shown in Figure 5. These conditions, in which continuous stress reversals were superimposed on a very slow loading rate, were more like periodic tidal loading of the Earth's crust than were the loading conditions shown in Figure 4. Stress oscillations in the experiments (~0.069 MPa) were significantly larger than typical Earth tide oscillations (0.001 to 0.004 MPa). Even so, no significant correlation was observed between the stress oscillations and the timing of stick-slip events. Measurable premonitory creep and the accompanying slip weakening can be seen 300 to 500 s before failure. Periodic oscillations in computed fault slip (Figure 6b) is the result of measurement noise.

express the model in terms of probability rather than seismicity rate by normalizing seismicity over a single cycle:

$$P(\theta) = P_0 + P_m \cos(\theta - \phi) \quad (4)$$

Here P_0 is the average value of the PDF and represents the uniform probability of the strictly Poissonian occurrence of events. Parameters P_m and ϕ are amplitude and phase shift, respectively, of the periodic component of the PDF corresponding to the part of the function that is correlated with the periodic loading signal. Since integration of the PDF over one cycle must result in unity probability, we have $P_0 = (2\pi)^{-1}$. Also, it is unlikely that the correlated portion of the PDF will be a pure sine wave. If the PDF were known exactly, it could be fit by standard Fourier series methods. Here, however, we are

Table 1. Experiment Summary

Series	N	V_r, μm/s	U_m, μm	τ_m, MPa	Frequency f, Hz	Period, s	1-P_{rw}	P_m/P_o	Phase ϕ, deg
A01	15	0.100	2.80	0.153	0.10	10	0.6890	0.52	-14
A02	27	0.100	5.40	0.265	0.10	10	0.9937	0.81	-38
A03	35	0.100	11.00	0.651	0.10	10	0.9999	1.08	-4
A04	22	0.100	1.39	0.099	0.050	20	0.3600	0.27	
A05	24	0.100	1.40	0.104	0.050	20	0.4932	0.33	
A06	23	0.100	2.80	0.189	0.050	20	0.5268	0.33	
A07	23	0.100	2.77	0.170	0.050	20	0.5370	0.34	
A08	16	0.100	5.50	0.381	0.050	20	0.9960	1.09	-18
A09	18	0.100	1.30	0.092	0.010	100	0.6110	0.42	
A10	15	0.100	2.73	0.183	0.010	100	0.9790	0.94	-17
A11	20	0.100	5.40	0.359	0.010	100	0.9963	0.98	-26
A12	10	0.100	5.50	0.359	0.010	100	0.9970	1.43	18
A13	23	0.100	2.70	0.171	0.0020	500	0.1371	0.22	
A14	25	0.100	5.40	0.342	0.0020	500	0.9969	0.89	-88
A15	17	0.100	11.00	0.711	0.0020	500	0.9999	1.51	-54
A16	31	0.100	0.00	0.000			0.5846	0.31	
B01	20	0.010	2.80	0.213	0.040	25	0.3888	0.29	
B02	27	0.010	5.50	0.272	0.040	25	0.9703	0.69	-68
B03	22	0.010	10.90	0.668	0.040	25	0.9984	1.01	-2
B04	24	0.010	1.30	0.089	0.0040	250	0.6666	0.41	
B05	19	0.010	2.70	0.168	0.0040	250	0.8061	0.55	23
B06	26	0.010	4.00	0.234	0.0040	250	0.6297	0.35	
B07	28	0.010	10.70	0.638	0.0040	250	0.9999	1.21	-7
B08	30	0.010	1.30	0.094	0.00043	2326	0.9618	0.58	-2
B09	19	0.010	2.70	0.178	0.00043	2326	0.9997	1.17	-14
B10	12	0.010	5.40	0.362	0.00043	2326	0.9994	1.51	7
B11	13	0.010	11.00	0.689	0.00043	2326	0.9991	1.17	-45
B12	20	0.010	2.70	0.172	1.0×10^{-4}	10000	0.9934	0.96	-15
C01	20	0.001	1.10	0.083	0.020	50	0.3398	0.27	

Series A10 and A12 were run at P_{conf} = 40 MPa; all others were run at 50 MPa. Series A16 was run at zero amplitude. For A16, correlations are shown for f = 0.05 Hz as an example. The test geometry provides the constraint: $CFF_m \approx 0.61\tau_m$. Phase angles ϕ are not listed for low-correlation series where phase uncertainties are large.

restricted by our limited event population to a rather crude estimate of the true PDF and can only expect to obtain useful information about the phase and amplitude of the fundamental frequency component. We also recognize that $P(\theta)$ is restricted to the interval $0 \le P(\theta) \le 1$; a condition which would be violated by (4) for P_m greater than P_0. We will defer until a later time the additional complexity in the model needed to correct for this condition since it only occurs in response to very large amplitude of the loading function.

Modeling of the stick-slip event catalogues involves two steps. First, the observed phases of the stick-slip events are used to construct an estimate of the true PDF. Because of the limited number of samples in each data set, the influence of each event is spread out using a cosine weighting function centered at the observed phase of the event. This smoothed probability estimate is then normalized so that when integrated over one cycle, the resultant total probability is unity. In the second step in the modeling, parameters P_m and ϕ

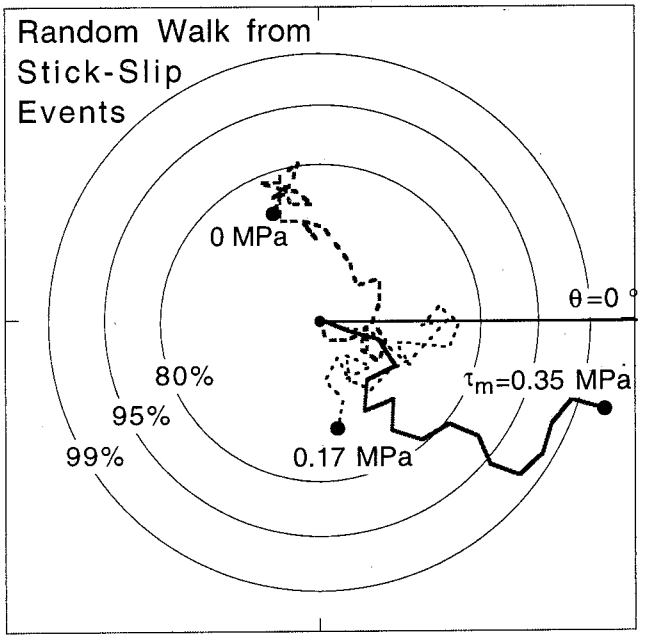

Figure 7. Examples of random walks using the phase of stick-slip event sequences from three experiments. Displacement oscillation amplitudes were 0, 2.8, and 5.5 μm (0, 0.17, and 0.35 MPa shear stress). Frequency of oscillation was 0.05 Hz. The largest amplitude stick-slip sequence showed a strong bias for events to occur with a phase of -20° (20° before peak stress). The possibility that this sequence of stick-slip events could occur by random chance can be rejected at the 99% confidence level. Both the zero amplitude and 2.8 μm sequences remained well within the limits expected for a random process. Presumably, a longer sequence of 2.8 μm amplitude events would begin to show a nonrandom drift similar to the 5.5 μm sequence.

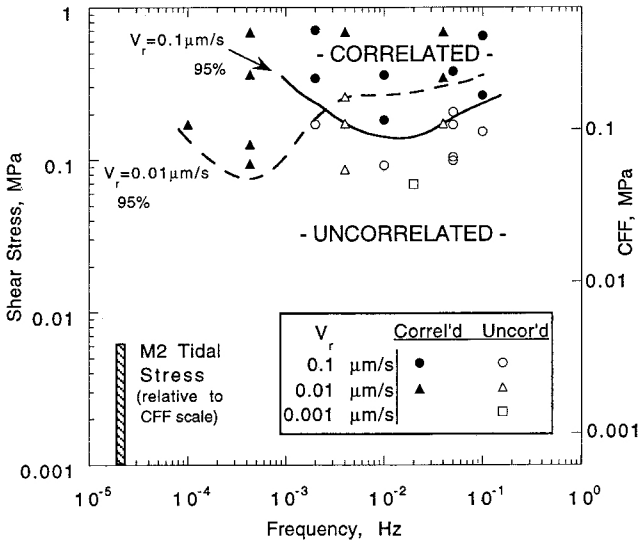

Figure 8. Log plot of frequency versus peak shear stress amplitude for the stick-slip sequences listed in Table 1 with remote loading rates V_r of 0.1 and 0.01 μm/s. Lines represent the 95% confidence interval for rejecting the null hypothesis that event sequences were the result of random chance. In all cases, large-amplitude oscillations produced correlated stick-slip events, and low amplitudes resulted in loss of correlation. A single uncorrelated sequence (series C01) at 0.001 μm/s is indicated by an open square.

are determined by a least squares method of fitting (4) to the estimated PDF.

Figure 9 shows model fits to the three examples discussed in section 3.2. The estimated PDF in the large-amplitude example (Figure 9a) shows an obvious correlation of stick-slip event timing with the peak amplitude of the periodic loading function. The peak in the PDF occurs at $\theta = \phi = -18°$, while the peak amplitude of the periodic loading function occurs at $\theta = 0°$. Therefore, in this example, peak seismicity precedes the peak in the periodic stress. The model fit, shown as the dashed line, captures most of the signal present in the estimated PDF. The two uncorrelated sets, at low and zero amplitude of the loading signal, are shown in Figures 9b and 9c. In both cases the estimated PDF is relatively featureless, and the resulting amplitude of the model fit is much smaller than in the strongly correlated example (P_m = 0.174, 0.051, and 0.050, respectively, in the three examples). Fluctuations in the estimated PDFs in Figures 9b and 9c cannot be distinguished from randomly occurring clustering of events, and the phase of the model fits has no significance in these examples.

A second set of measurements with oscillations of period 25 s is shown in Figure 10. Both the 0.69- and 0.35-MPa series show significant correlation of stick-slip events. As loading signal amplitude decreases, a corresponding decrease in amplitude of the model response function occurs. Input amplitudes of 0.69, 0.35, and 0.17 MPa correspond to response amplitudes P_m of 0.160, 0.109, and 0.046, respectively. Listed in Table 1 are the ratios P_m/P_0 representing the amplitudes of the correlated response normalized by the average or random component of the probability model. Values greater than one indicate that the correlated response dominates the occurrence of stick slip events. Small values of P_m/P_0 indicate conditions under which only a weak correlation exists between the periodic loading function and the occurrence of stick-slip events.

Figure 11 shows the result of a series of Monte Carlo simulations of purely random, uncorrelated stick-slip event times. Figure 11a shows four examples of estimated PDFs based on 20 event sequences. These examples show significant variations from the true PDF (with constant probability P_0 = 0.1592). Clearly, samplings of 20 events are not sufficient to guarantee resolution of any subtle features in the true PDF. Figure 11b shows the estimated PDF resulting from a 200-event sampling. This simulation has provided significant improvement in recovering the true PDF. Monte Carlo simulations of 20 event sequences suggest that normalized amplitude ratios $P_m/P_0 < 0.4$

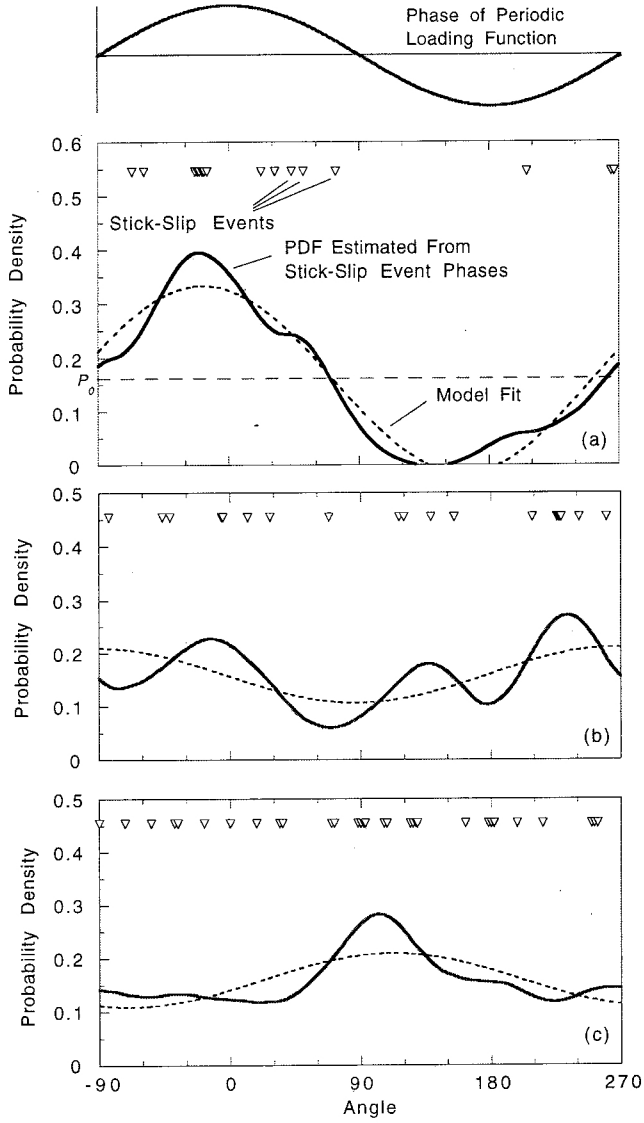

Figure 9. Stick-slip event phases (triangles) for the three event sets shown in Figure 7. Solid line in the lower portion of each graph is the estimated probability density function (PDF) reconstructed from smoothing of the stick-slip event times. The dashed line in each graph is the least squares fit of equation (4) to the estimated PDF. (a) The well correlated sequence produces a large sine wave component to the fit, while (b) and (c) the poorly correlated sequences have much smaller sine wave components. Parameter fits are listed in Table 1.

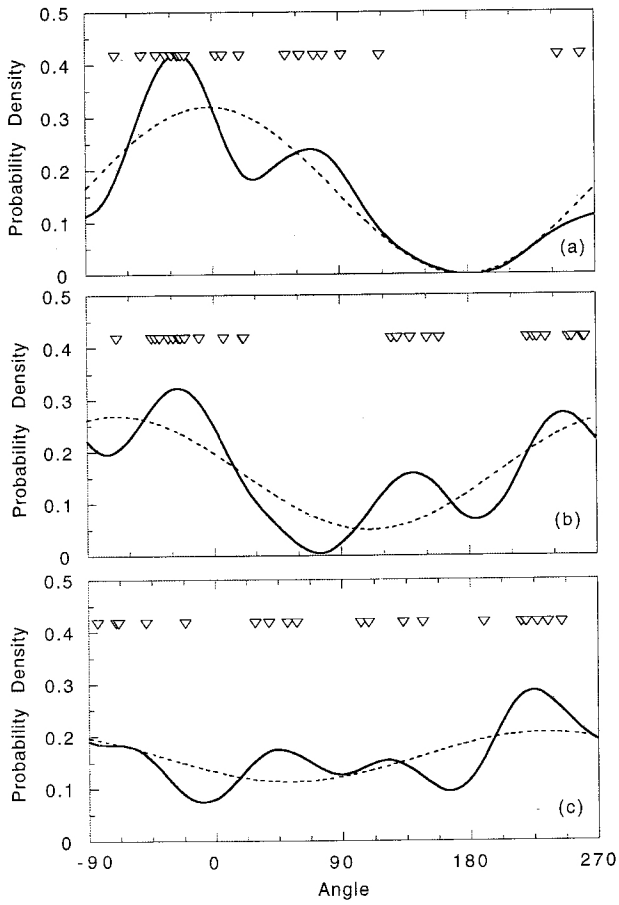

Figure 10. Stick-slip event phases for V_r = 0.01 μm/s and a forcing function period of 25 s. Forcing function amplitudes are 10.9, 5.5, and 2.8 μm (0.69, 0.35, and 0.17 MPa shear stress, respectively). Decreasing forcing function amplitude results in a systematic loss of event clustering and decline in the sine wave component of the model fit. As in Figure 9a, the peak in the stick-slip activity precedes the peak in the forcing function.

cannot be distinguished with confidence from purely random event sequences. Consequently, we have plotted in Figure 12 contours of P_m/P_0 equal to 1.0 and 0.5. Values smaller than this can, in principle, be obtained from experiment sequences recording greater numbers of stick-slip events. The shape of the contours are similar to the shape of the 95% confidence contours drawn in Figure 8. By decreasing the remote loading rate, the minimum in the contours is shifted to lower amplitude and lower frequency. Reducing the amplitude of the forcing function by a factor of 2 results in a similar reduction in the correlation ratio, implying that the level of correlation is approximately proportional to the amplitude of the forcing function.

4. Fault Simulations

4.1. Basic Characteristics

One long-term goal of this study is to explain laboratory and field observations of time-dependent failure and triggered seismicity in terms of fundamental physical processes. At present, however, we will limit the scope of our analysis by comparing the laboratory observations to predictions of existing end-member theoretical earthquake failure models. This exercise may also provide clues as to how our observations could be extrapolated to natural loading rates, cyclic stress amplitudes, and periods. To model the laboratory earthquake catalogues we must first consider characteristics of candidate failure models when steady loading rates without oscillatory components are applied. We assume, consistent with (4), that the laboratory stick-slip event populations consist of a purely random component and a component that responds to the periodic loading signal. We have tested this assumption (series A16 in Figure 9c) by running a sequence of stick-slip events at constant loading rate without a periodic loading signal. The resulting PDF cannot be distinguished from random over the range of frequencies considered here. The observed phase of these stick-slip events occurs randomly, requiring that for vanishingly small oscillating stress amplitude, simulated event catalogues should also contain random failure phases. This random component in the model population must be generated artificially in our numerical simulations because the numerical failure models that we consider are deterministic; that is, under constant loading the failure events are all identical with constant interevent time, failure stress, stress drop, etc. To make the unperturbed simulated populations fail at random phases the stresses at the start of the simulations are distributed randomly within a stress range $\Delta\tau = kV_r/f$, where k is stiffness, V_r is loading velocity, and f is the frequency of interest (angular frequency $\omega = d\theta/dt = 2\pi f$) of the oscillating stress. We proceed under the assumption that the fault properties which respond to the periodic loading are independent of the properties or circumstances which lead to P_0.

4.2. Coulomb Failure Model

The first failure model that we will consider is based on the well-known Coulomb failure condition in which failure occurs

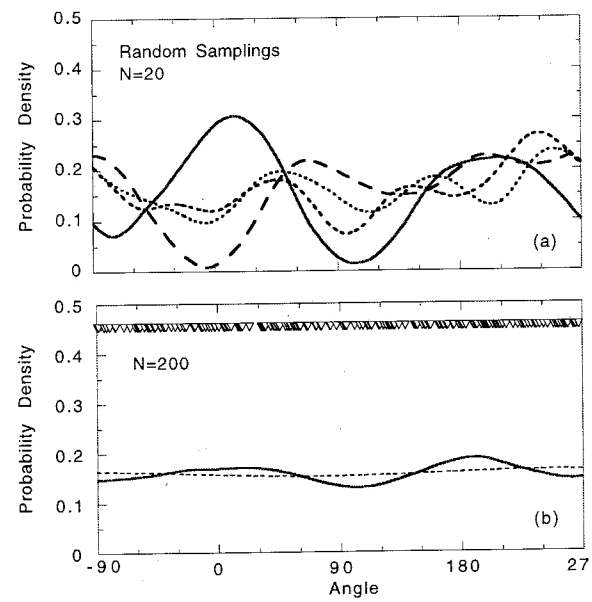

Figure 11. (a) Estimated PDFs derived from four synthetic sets of 20 random event phases. The true PDF from which the samples were taken has uniform probability of $(2\pi)^{-1}$. (b) Estimated PDF (solid line) resulting from a sampling of 200 random events (shown as triangles). True PDF is shown as dashed line. A factor of 10 increase in event population provides an obvious improvement in the estimated PDF.

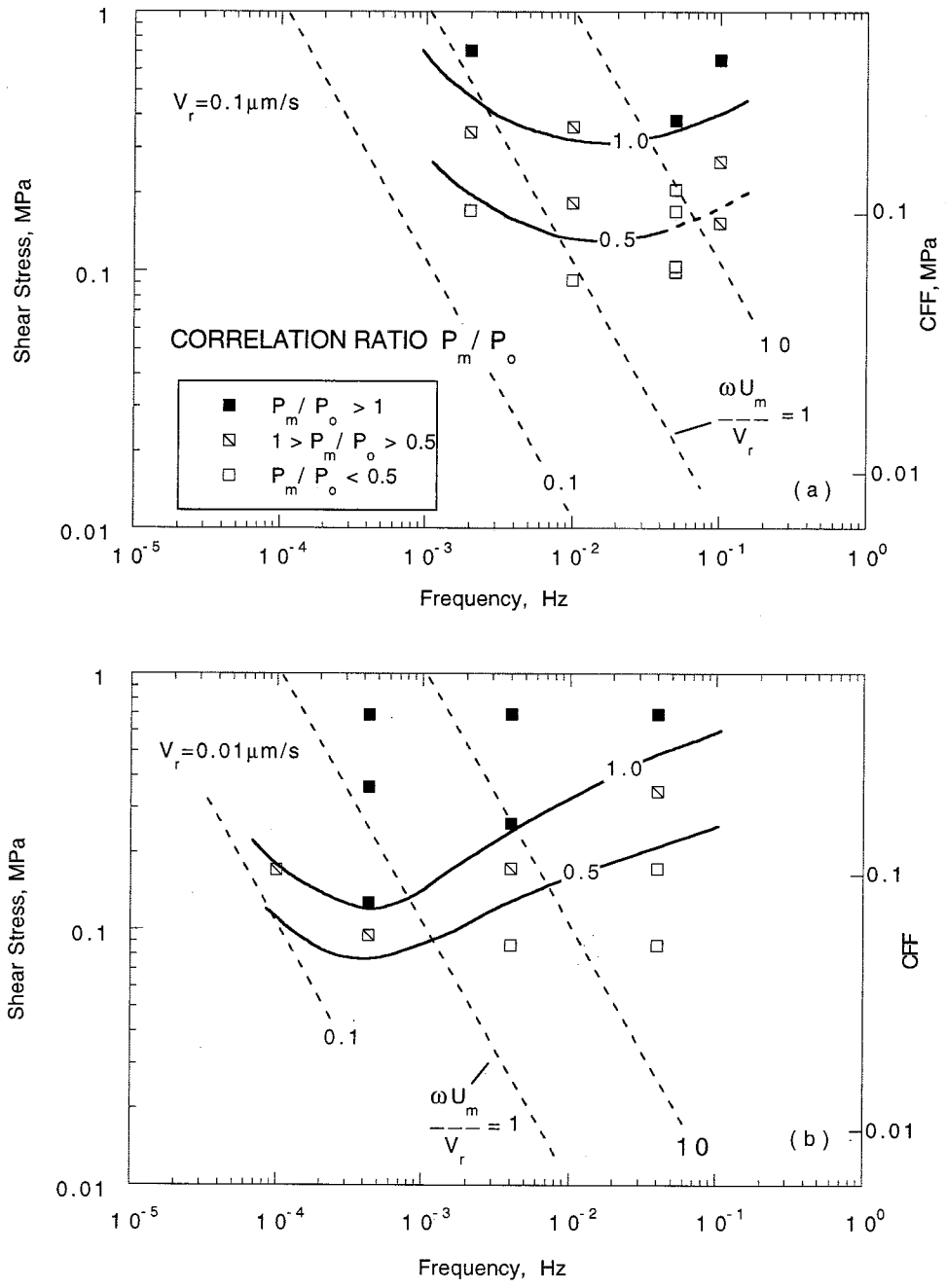

Figure 12. Contours of P_m/P_o = 1.0 and 0.5 for experiment sets with (a) V = 0.1 μm/s and (b) V = 0.01 μm/s. Tidal stresses, in the 0.001 to 0.004 MPa range, are well below the amplitudes needed to produce correlated earthquakes according to these plots. Some aftershock sequences show good correlation with regions of calculated stress increases above 0.01 to 0.05 MPa, in general agreement with the threshold we observe. Remote triggering of earthquakes because of passage of surface waves as in the Landers earthquake generally occurred for stress amplitudes above 0.1 MPa at frequencies of 0.05 to 0.2 Hz [*Hill et al.*, 1993], as might be expected from the laboratory data shown here.

abruptly when an increase in shear stress τ and/or decrease in normal stress σ_n leads to the yield condition expressed by (2). In this case both C and μ are assumed to be constant. Given a large population of events and provided that the maximum loading rate of the oscillating signal does not exceed the steady background loading rate V_r, the expected degree of correlation of populations obeying (2) can be calculated in a straightforward manner.

All numerical models were run at constant normal stress, thereby simplifying the analysis without significant loss of generality. Failure occurs in each simulation at the same value of shear stress, and the instantaneous event rate R is proportional to load point displacement rate $V_L = du_L/dt$ at the time of failure.

In both the laboratory experiments and the numerical simulations, the periodic loading function has the form

$$u_m = U_m \cos(\omega t), \quad (5)$$

where u_m is the modulated displacement component at the control point with amplitude U_m. As a result, the velocity at the control point, including the long-term loading rate, becomes

$$V_L = V_r - \omega U_m \sin(\omega t). \quad (6)$$

The relative event rate becomes $R(\theta)/R_{av} = V_L(\theta)/V_r$, where R_{av} is the average event rate. In this mode of response the maximum event rate coincides with the maximum loading rate (*i.e.*, $\theta_{R=\max} = -90°$), preceding the peak in the stressing function by 90°. Figures 13c and 13d show examples of this loading regime for numerical simulations of 100 stick-slip events. These simulations use V_r = 0.01 μm/s and an oscillation period of 25 s which are similar to the conditions of experiments B01 to B03 (Figure 10). As expected, the phase shift of the maximum seismicity rate is $\phi \sim -90°$.

If the maximum periodic loading rate exceeds the background loading rate, a condition which occurs when $\omega U_m/V_r > 1$ (Figure 14a), strong correlations with the oscillating loading function will result and the maximum event rate can occur in phase with the peak stress ($\theta_{R=\max} \sim 0°$). This can be understood as follows: when the maximum periodic loading rate exceeds the background loading rate, the net loading rate becomes negative for some portion of each cycle (Figure 14b). Because (2) represents a failure threshold, failure cannot occur until the stress exceeds the peak stress of the previous cycle. Using a Coulomb failure criterion, there are no events between θ_{peak} and θ_{emerge}. (Figure 14b). This notion has a counterpart referred to as the Kaiser effect in acoustic emission studies [*Holcomb,* 1993; *Lockner,* 1993]. As amplitude or frequency increases, θ_{emerge} increases, and once it exceeds 270°, because the relative number of events still correlates with the loading velocity, $\theta_{R=\max} = \theta_{emerge}$. Under these conditions $\theta_{R=\max}$ can shift to higher phase as shown in the simulations plotted in Figures 13a and 13b. For a shear stress amplitude of only 0.0072 MPa (Figure 13a) the stress shadow from one cycle to the next spans about 230° during which no stick-slip events occur. In addition, the maximum seismicity rate no longer occurs at -90°, but rather, it approaches the phase of peak stress ($\theta_{R=\max}$ = -70° in Figure 13a).

In the case of tidal loading, the quantity $\omega U_m/V_r$ is much greater than 1 and stress at each cycle only emerges from the previous cycle for a brief period near $\theta = 0°$. Thus, based on a Coulomb failure model, the standard expectation for correlation of earthquakes with Earth tides is a coincidence of peak loading stress with peak earthquake activity. Furthermore, in the absence of competing effects, essentially all earthquakes should show a temporal correlation. As we noted in section 1, this in fact is the case for moonquakes [*Lammlein et al.,* 1974]; a case where Coulomb failure may be an appropriate model.

Given the specific predictions of (2) it is easy to evaluate the consistency of Coulomb failure with the experimental data. We find that, in general, the agreement is poor. Seismicity becomes strongly correlated at a shear stress amplitude of approximately 0.0018 MPa (Figure 13c) or displacement amplitude U_m = 0.03 μm. These conditions correspond to $\omega U_m/V_r = 0.8$ in agreement with the expected transition from uncorrelated to correlated events discussed above. While the shift in phase with increasing amplitude may be consistent with at least some of the laboratory observations, the stress level at which the transition from uncorrelated to correlated events occurs is nearly 2 orders of magnitude below the level observed in the experiments (Figure 12b). This lack of agreement with the laboratory data is indicative of the inadequacies of a failure model that lacks time dependence.

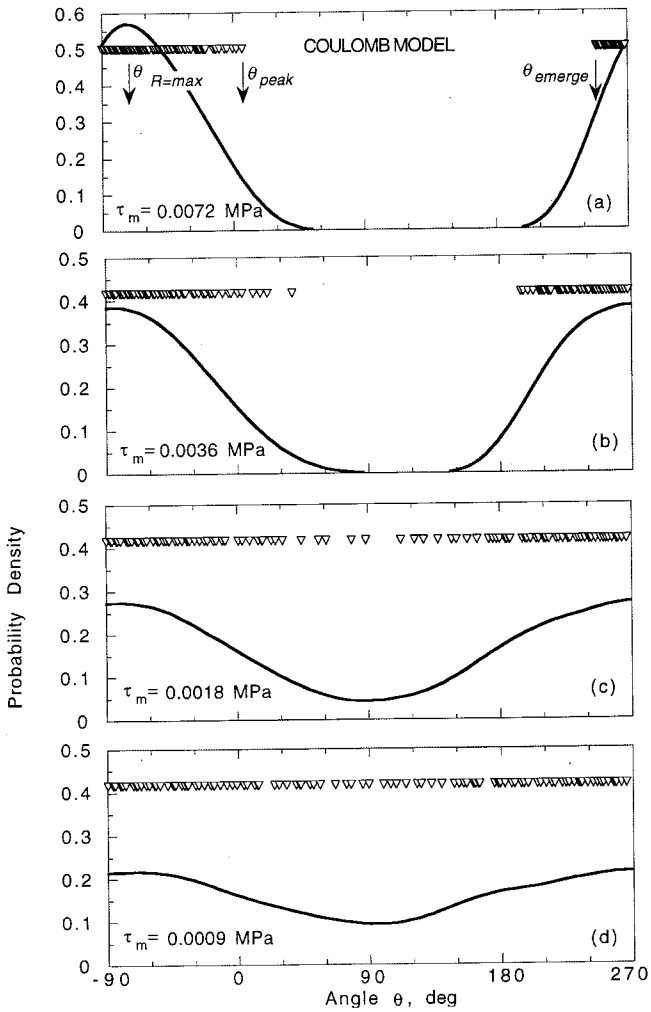

Figure 13. Estimated PDFs for numerical simulations of 100 stick-slip events based on Coulomb yield condition (equation 2) and modeling as described in section 4.2. Run parameters were similar to conditions for experiments in Figure 10: V_r = 0.01 μm/s, σ_n = 85 MPa, μ = 0.7, k = 60.35 MPa/mm, f = 0.04 Hz, and modulated shear stress amplitudes of τ_m = (a) 0.0072, (b) 0.0036, (c) 0.0018, and (d) 0.0009 MPa, respectively. Simulations show a steady increase in correlated seismicity with increasing amplitude of the stressing function. Low-amplitude simulations in Figures 13c and 13d show maximum seismicity rate preceding the peak in shear stress (ϕ = -90°). For $\omega U_m/V_r > 1$ (Figures 13a and 13b), a stress shadow occurs each cycle in which no stick-slip events occur. With increasing amplitude (Figure 13a), the phase shift ϕ begins to approach zero. These properties are characteristic of a yield condition which involves instantaneous failure. Stress amplitude for transition from uncorrelated to correlated seismicity is approximately 2 orders of magnitude less than the amplitude observed in the experiments.

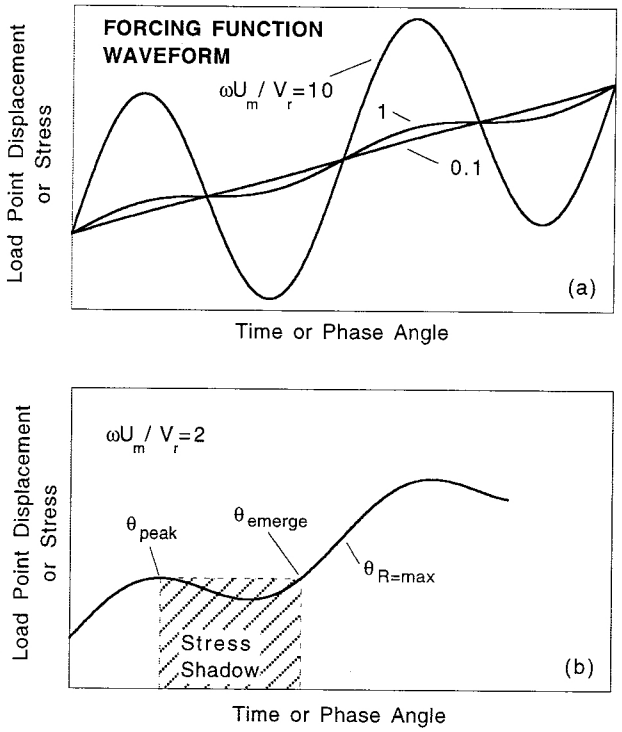

Figure 14. The waveform of the forcing function satisfying equations (5) and (6) is controlled by the quantity $\omega U_m/V_r$ which expresses the relative strengths of the oscillating component and the constant long-term loading rate component. (a) Correlation of seismicity with the oscillating component very weak for $\omega U_m/V_r$ less than about 0.1. For diurnal tidal loading this quantity exceeds 100, suggesting that a strong correlation should occur. The lack of strong tidal triggering implies that a different mechanism, presumably involving delayed failure, controls the timing of earthquakes under the conditions of lunar tidal stressing. (b) The forcing function where amplitude of the oscillating stress is large enough to cause periodic reversals. A Coulomb failure model predicts that no failures can occur during the stress shadow region in which the stress level has previously been exceeded.

4.3. Rate-Dependent Failure

The laboratory experiments show delayed failure involving precursory slip lasting hundreds of seconds and failure that is not abrupt (Figure 4). These characteristics are inconsistent with a threshold failure model such as the Coulomb model that has no time dependence built in. Furthermore, based on the observations from numerous studies of rock friction [*Dieterich,* 1981; *Tullis and Weeks,* 1986; *Blanpied et al.,* 1998] and failure of intact rock [*Lockner,* 1998], strength is expected to depend instantaneously on the logarithm of the rate of inelastic deformation, as well as undergo gradual failure. When rate dependence is positive, so that increased deformation rate leads to increased strength, the tendency is to stabilize and delay failure.

Numerical simulations reported by *Dieterich* [1987] involved a single degree of freedom spring and block model using fault constitutive equations

$$\mu = \mu_o - A_1 \ln\left(A_2 \frac{D_c}{V} + 1\right) + B_1 \ln(B_2 \psi + 1) \qquad (7)$$

$$\frac{d\psi}{dt} = 1 - \psi \frac{V}{D_c}, \qquad (8)$$

where A_1, A_2, B_1, and B_2 are experimentally determined parameters, V is fault slip rate, ψ is a time-dependent state variable, and D_c is a characteristic slip-weakening distance. We will discuss Dieterich's modeling results in section 5. For our own initial modeling efforts we have chosen a simpler constitutive equation that, nevertheless, highlights the differences between the non-rate-dependent Coulomb model and a model that includes time-dependent (or in this case displacement-dependent) weakening. The constitutive equation we use,

$$\mu = \mu_o + A_1 \ln \frac{V}{V_o} - B_1 \frac{u}{D_c}, \qquad (9)$$

exhibits log rate dependence, precursory slip and weakening and has the advantage that near failure is fairly consistent with the predictions of laboratory based frictional constitutive equations [*Dieterich,* 1992]. Equation (9) is a simplification to (7) and (8) as used by *Dieterich* [1987], under the conditions $A_2D_c/V > 1$, $\psi B_2 > 1$, and $\psi V/D_c > 1$. The first two conditions are the velocity cutoffs on rate and state effects (e.g., *Okubo and Dieterich* [1986]). On the basis of previously published experimental data for granite at high normal stress, the cutoffs come into play only at higher velocity than we consider in our modeling (i.e., for $V > 1$ mm/s [*Kilgore et al.,* 1993]). The third criteria is satisfied when the sliding velocity approaches the loading rate, typically during the onset of significant precursory slip. Thus, near failure, (9) is a good approximation of (7) and (8).

For an oscillatory loading function coupled through an elastic element ($\tau = k(u_L - u)$) to a fault with frictional strength satisfying (9), there is no analytical solution for fault motion. Consequently, we have solved these equations numerically with a Runga-Kutta scheme. The starting conditions of stress are as described in section 4.1, and the starting sliding velocity is determined from the starting stress assuming $u = 0$ initially. Because with (9) failure is not abrupt, we have arbitrarily defined failure as occurring when the sliding velocity reaches a threshold level of 1 mm/s. Since slip is accelerating rapidly by this point, choice of a higher slip rate threshold does not significantly change the modeling results. The distributions of simulated stick-slip events, shown in Figure 15, are similar to the laboratory data (i.e., Figure 10), and compared to the Coulomb model, they do a better job of matching the amplitude at which the correlation of seismicity becomes strong. There is essentially no phase shift ($\phi \sim 0$) between the peak seismicity rate and the peak stress amplitude for all conditions studied. While a clear trend was not identifiable in the phase data obtained from the laboratory measurements, some sequences showed clear evidence of peak seismicity rate preceding peak stress (Figures 7 and 9a).

5. Discussion

Earlier analyses of the possible connection between Earth tides and the timing of earthquakes have typically searched for statistical correlations in earthquake catalogues. If, indeed, a correlation exists, it appears to be a small fraction of the dominant random (or at least uncorrelated) occurrence of earthquakes [*Vidale et al.,* 1998b]. One possible exception is the observation by *Kilston and Knopoff* [1983] that large-

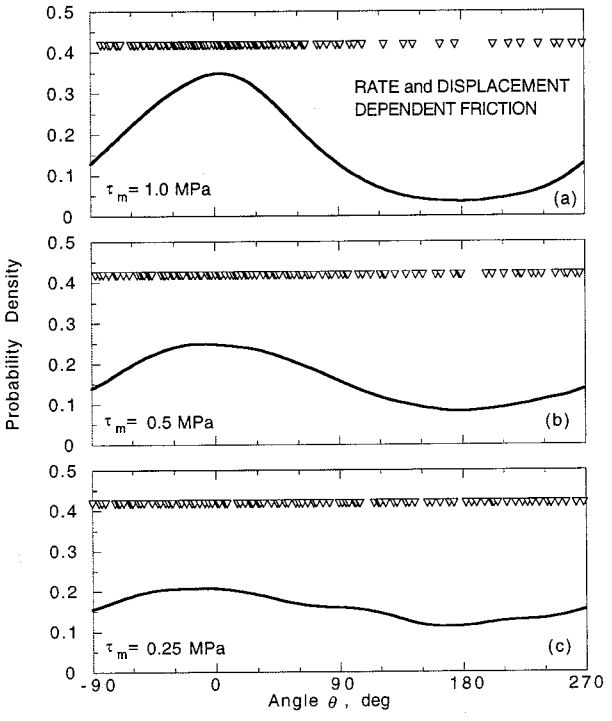

Figure 15. Estimated PDFs for numerical simulations of 100 stick-slip events based on a rate- and displacement-dependent fault rheology (equation (9)). Model parameters are the same as in Figure 13 with the addition of $a = A_1/\sigma_n = 0.01$, $b = B_1/\sigma_n = 0.01$, and $D_c = 1$ μm. Modulated shear stress amplitudes were τ_m = (a) 1.0, (b) 0.5, and (c) 0.25 MPa. Amplitude where seismicity becomes correlated is similar to experimental results.

magnitude southern California earthquakes show correlations to different solar and lunar periodicities. While a set of 22 smaller earthquakes ($5.3 \leq M \leq 5.9$) showed no significant correlations, the 13 largest events ($M \geq 6$) did show what they claimed were statistically significant correlations. We have applied the Schuster test (equation (3)) to the diurnal phases shown in Figure 3a of *Kilston and Knopoff* [1983] and found a correlation at only the 88% confidence level. Kilston and Knopoff applied a χ^2 test and rejected the uncorrelated event null hypothesis at the 95% level. By the standards that we have applied to our laboratory data (Figure 8), an 88% confidence level for a single data set would be considered ambiguous.

In the present study we have attempted to identify the range of amplitudes and frequencies of simple sinusoidal forcing signals that result in correlated model earthquakes (referred to as stick-slip events in laboratory friction studies). The result, best summarized in Figure 12, spans approximately 1 decade in amplitude of the forcing signal and 3 decades in frequency. The peak shear stress in these experiments is nominally 56 MPa (Figures 3, 4, and 5), and the constraints of the loading system control are such that ±0.05 MPa represents a practical lower limit to the amplitude of the shear stress oscillations. Maximum tidal stressing amplitudes in the shallow to midcrust are calculated to be in the 0.001 to 0.005 MPa range [*Melchior,* 1983; *Vidale et al.,* 1998b] at periods of 4.5×10^4 s (12.5 hours) and 1.2×10^6 s (14 days). In the present study we have investigated periods from 10 s up to 10^4 s. While some scaling is necessary to extrapolate our results to Earth tide conditions, we actually overlap the range of teleseismic amplitudes and periods as well as stress step amplitude and duration calculated for earthquake aftershocks. At higher frequencies our observations also border on the range of stress oscillations in the near and intermediate field because of passage of body and surface waves [*Hill et al.,* 1993; *Anderson et al.,* 1994; *Gomberg and Davis,* 1996]. These different naturally occurring phenomena, which are generally considered separately, should be considered together. Furthermore, these phenomena, as well as our own laboratory observations, can be broadly grouped into three regions, namely, (1) strongly correlated seismicity at large amplitude of the forcing signal, (2) uncorrelated seismicity at low amplitude, and (3) a transition region where weak correlation may exist. We also support the suggestions of previous studies that favorable conditions may enhance the level of correlation, that is, the presence of fluid-filled cracks, regions of low rigidity, low effective normal stress, or high background seismicity rate.

One important limitation of our study is that we have not determined the effect of varying average normal stress on the level of correlation between forcing function amplitude and earthquake timing. We anticipate that at least to first order the amplitude of shear stress variations needed to produce earthquake correlations will be proportional to the applied effective normal stress acting on the fault surface. Consequently, variations in coefficient of friction μ rather than shear stress will be roughly independent of normal stress. This relation, which has not yet been experimentally verified, was suggested by *Dieterich* [1987] based on a particular rate- and state-dependent fault rheological model. In fact, Dieterich's analysis anticipated a number of findings of the present study and warrants particular attention. The numerical simulations reported by *Dieterich* [1987] involved a single degree of freedom spring and block model using fault constitutive equations (7) and (8). Dieterich reported on numerical simulations for sinusoidal stress perturbations in a spring-block model using periods of 12.5 hours (diurnal tidal period) and 1 year. To summarize his results, Dieterich plotted seismicity rate R normalized by the average seismicity rate R_{av}. While he did not refer to it as such, this parameter is equivalent to the estimated PDFs that we have shown in Figures 9, 10, and 11. His parameter R_a quantifies the relative strength of the correlated seismicity response. If the correlated seismicity response were a pure sine wave, we would have, in fact,

$$\frac{R_a}{2} = \frac{P_m}{P_0} . \tag{10}$$

Dieterich [1987] reported that in his simulations, correlations between the forcing function and the timing of earthquakes were independent of D_c, spring stiffness, remote loading rate, A_2, B_1, and B_2, as well as the period of the forcing function. He observed no measurable phase shift between the forcing function and the earthquake response (i.e., instabilities tended to cluster at the peak in the loading cycle). He found that the seismicity response was linear in the sense that R_a was proportional to amplitude of the stress forcing function. Also, he reported R_a inversely proportional to the constitutive parameter A_1, implying

$$\frac{R_a}{2} = \frac{\tau_m}{A_1 \sigma_n} \cong \frac{P_m}{P_o} , \tag{11}$$

where τ_m is the amplitude of the periodic shear stress forcing function. These are very specific findings, and while we have not tested all of them, we do have results that bear directly on some of these predictions. Mainly, we have varied remote loading rate and period of the modulating signal and find that the degree of correlation of seismicity (P_m/P_o) is dependent on both of these parameters. For example, at a period of 100 s (Figure 12), increasing the loading rate by a factor of 10 decreases the stress amplitude for correlated seismicity by a factor of 2. Also, the frequency dependence of the correlation contours in Figure 12 is significant. For both remote loading rates, contours pass through a distinct minimum. Across a span of 3 decades in frequency the correlation response varies by a factor of 2 to 4. The rise in the correlation contours at the longest periods is apparently outside of the range of parameter space considered by Dieterich.

Given the limited range of correlation response that we are able to determine using samplings of 20 stick-slip events, we find that the level of correlation scales approximately linearly with the amplitude of the driving stress. This important finding agrees with Dieterich's numerical simulations. We can also test the validity of (11) by applying values shown in Figure 12. For $P_m/P_o = 1$, we find that τ_m ranges from 0.15 to 0.5 MPa with a normal stress of approximately 82 MPa. Taking into account the accompanying change in normal stress for a fault inclined 30° to the sample axis, the corresponding change in coefficient of friction as well as the range of predicted values of A_1 based on (11) spans values from 0.001 to 0.004. This overlaps the range of laboratory reported values for A_1 of about 0.003 to 0.009 for dry Westerly granite [*Blanpied et al.*, 1998]. Given the simplicity of Dieterich's numerical model and the difference in test conditions between this study and the studies used to measure A_1, we consider this level of agreement to be a validation of this conceptual approach.

Of the various observations reported in this study, the phase shift ϕ between the seismicity response and the forcing function is probably the least well constrained. It is possible that the interaction of the premonitory creep with the oscillating forcing function may result in measurable phase shifts. We have noted that for low correlation levels ($P_m/P_o <$ 0.5), phase information will be unreliable. The observed phase shifts for the better correlated sequences suggest a possible dependence on frequency and amplitude of the forcing function. However, the data seem too inconsistent to make reliable associations at this time. The average and standard deviation of the phase data listed in Table 1 are $\phi = -20° \pm 29°$. Thus there is a tendency for clustering of earthquakes before the maximum in the periodic forcing function, but this phase shift does not happen consistently and is not statistically significant.

In the present study we have not tested the mean normal stress dependence of the correlated seismicity. As pointed out by *Dieterich* [1987], this relation is important for understanding how induced seismicity may vary with depth. From his analysis, as effective normal stress increases, the change in shear stress needed to produce the same level of correlated seismicity will be proportionately larger. A possible method for testing this hypothesis might be to look at the depth dependence of aftershocks and how they are correlated to estimated changes in stress level. It is interesting to note that at present, no depth or frequency dependence has been reported in studies of triggered seismicity. In all cases a threshold of either stress or strain has been proposed. *Anderson et al.* [1994] found that seismicity, apparently triggered by passage of dynamic stress waves from the $M_w = 7.3$ Landers earthquake, occurred in the western Basin and Range province in regions of high background seismicity. They concluded that peak amplitude of the dynamic waves needed to exceed 0.6 to 0.9 MPa at periods of 10 s or greater to induce secondary earthquakes in these regions which were presumably in a condition of incipient failure. Our laboratory data (Figure 10) are fully consistent with this conclusion. *Hill et al.* [1993] also looked for correlations between post-Landers induced seismicity and calculated stress amplitudes of radiated surface waves. They noted that some seismically active geothermal areas in particular showed increased seismicity if dynamic stress wave amplitudes exceeded 0.1 to 0.2 MPa at periods of 5 to 20 s. Finally, *Gomberg and Davis* [1996] argued that at The Geysers, California, an increase in seismicity could be associated with passage of dynamic waves with strain amplitudes exceeding approximately 0.1 to 0.4 μstrain. For a representative shear modulus of 30 GPa we expect a shear stress threshold of about 0.003 to 0.012 MPa. While this threshold is smaller than the level inferred by *Anderson et al.* [1994] for western Basin and Range induced seismicity, triggered events at The Geysers are generally shallow (1 to 2 km) and therefore at lower normal stress. Thus there may be some sensitivity to normal stress hidden in the available field data.

The strongest and most significant result shown in Figures 8 and 12 is that we identify a region, at large amplitude of the periodic forcing function, in which model earthquake occurrence is influenced by the stress oscillations. As the amplitude of the forcing function is reduced, the correlation of earthquake timing systematically disappears. While the P_m/P_o = 0.5 contour in Figure 12 is approaching the resolution limit for our measurements, it appears that the loss of correlation drops off linearly with forcing function amplitude. The loss of correlation occurs at roughly 0.1 MPa (1 bar) shear stress or 0.06 MPa ΔCFF as discussed in section 3.1. Since normal stress is changing with shear stress in these experiments, the change in Coulomb stress (or alternatively, the change in coefficient of friction) may be a better measure of the stress sensitivity. As discussed in section 3.1, a 0.1-MPa increase in shear stress represents approximately 0.06-MPa increase in Coulomb failure stress (or 0.0007 increase in coefficient of friction). If this effect scales linearly with normal stress, then the experimental conditions of 50 MPa confining pressure represent a burial depth for dry granite of approximately 2 km. Assuming hydrostatic fluid pressure, this effective confining pressure is more representative of about 3 km depth.

The increase in the correlation contours at long periods can be understood by considering the interaction of the long-term loading rate V_r and the periodic signal at these conditions. The displacements imposed in these experiments were discussed in section 4.2 (equations (5) and (6)). For small-amplitude oscillations the loading rate is essentially V_r, and the periodic forcing function will have no influence on the timing of stick-slip events (Figure 14a). In the absence of other effects the modulating displacement function should begin to influence the timing of stick-slip events once the maximum periodic rate is comparable to the long-term loading rate:

$$\frac{\omega U_m}{V_r} = 1. \tag{12}$$

When (12) is satisfied, loading rate at the control point will vary each cycle from 0 to $2V_r$. Lines parallel to (12) are plotted

as dashed line in Figures 12a and 12b. Given the change in character of the forcing function as shown in Figure 14a, we would expect to see a loss of strong correlation for values of $\omega U_m/V_r$ between 0.1 and 1. This criterion implies an approximate boundary between correlated and uncorrelated regions with a slope of ω^{-1} and which shifts as $1/V_r$. This theoretical transition matches the low-frequency data reasonably well, although more measurements would be needed to rule out other possible frequency dependence. We have already noted that (12) provides a good criterion for predicting the level of correlation resulting from the Coulomb failure model. The fact that both remote loading rate data sets appear to contain a minimum as shown in Figure 12 indicates that for higher frequencies a different mechanism is responsible for the loss of correlation between forcing function and seismicity. We suggest that this mechanism is related to premonitory slip as discussed here and elsewhere [*Vidale et al.,* 1998b].

We believe that understanding the delayed failure which is common to the experiments in this study and observations of static fatigue in failure of rocks [*Kranz,* 1980; *Lockner,* 1998] and other brittle materials [*Wiederhorn and Bolz,* 1970] is the key to determining the stress sensitivity of failure in the Earth. Qualitatively, sensitivity to periodic stress arises when the modulating stress induces a significant change in the duration of the delay. There are many ways in which this might occur. As discussed in section 3 in this paper and by *Dieterich* [1987], we suggest that premonitory slip which accompanies the delay and defines the gradual onset of failure is also implicated in the loss of correlation between the periodic stress and failure time for certain combinations of amplitude and frequency. For example, if failure occurs at a critical amount of precursory slip, correlation of failure with the oscillating stress arises when the positive portion of the oscillating driving stress is large enough to significantly increase the sliding velocity during precursory slip above the average velocity. Such an increase in sliding velocity is equivalent to a reduction in the delay time to failure and leads to a correlation which has a natural dependence on stress amplitude and frequency. Phase shifts between the forcing function and the seismicity should also be expected under certain conditions.

If resolving power of the statistical approach discussed in sections 3.2 and 3.3 improves as $\sqrt{N}$ (see the appendix) and if the level of correlated seismicity varies linearly with amplitude of the stress oscillations, we can extrapolate the correlation levels shown in Figure 12 to Earth tide levels. If a sampling of 20 earthquakes is needed to resolve the $P_m/P_o = 0.5$ correlation contour at a shear stress level of about 0.1 MPa, we expect that for tidal stresses of 0.003 MPa we would require a minimum sample size of approximately 20,000 earthquakes to detect a statistically significant correlation. This would correspond to a correlation level of $P_m/P_o \sim 0.015$. *Vidale et al.* [1998b] have reported no significant correlation for a set of 13,042 earthquakes which is consistent with our extrapolation. More recently, from work in progress *Vidale et al.* [1998a], have reported a weak correlation (i.e., $P_m/P_o \sim 0.01$) using a catalogue of 27,464 earthquakes. This apparent agreement between laboratory and field observations is encouraging.

Our own explanation for the occurrence of correlated seismicity is based on laboratory observations. We suggest that the lack of observed tidal triggering indicates that the timing of failure of natural faults is controlled by the amplitude and frequency content of the driving stress. A correlation between stress path (stress history) and failure time is expected if the rheology of the Earth's crust is similar to other brittle materials which permit delayed failure.

6. Conclusions

In this study we have conducted laboratory simulations of earthquake sequences in which the remote loading condition was a constant deformation rate modulated by a small-amplitude sine wave. At shear stress amplitudes above approximately 0.1 to 0.4 MPa we have observed a strong correlation between the periodic forcing function and the occurrence of model earthquakes. In many cases the peak in the induced seismicity preceded the peak in the forcing function. As the amplitude of the forcing function decreased, the correlation of timing of the induced seismicity also decreased.

In recent years a variety of phenomena have been considered which attempt to relate transient or periodic loading of the Earth's crust to triggered seismicity. The natural forcing functions include solid Earth tides, reservoir impoundment, and dynamic and static stress changes caused by large earthquakes. These phenomena, as well as our own laboratory observations, can be broadly grouped into three regions: (1) For modulated signal amplitude greater than about 0.1 MPa (1 bar) shear stress (or 0.06 MPa Coulomb failure function), earthquake occurrence is strongly correlated with the forcing function. (2) For amplitudes below 0.01 MPa, little or no correlation can be detected. (3) Shear stress variations between 0.01 and 0.1 MPa represent a transition region in which correlation of earthquake occurrence may occur; especially for some favorable geometries. These geometries might include, for example, regions of high fluid pressure or active geothermal or volcanic areas or zones of low effective normal stress. Our experimental results indicate that conditions needed for correlated seismicity do depend to some degree on the frequency content of the forcing function as well as on the long-term loading rate. Future studies of this type should include testing of normal stress dependence as well as the effect of slower long term loading rates. The present results were carried out at 50 MPa confining pressure which, for normal hydrostatic and lithostatic pressure gradients, corresponds to approximately 3 km depth. Weaker seismicity correlations than what were determined in this study could be achieved by sampling larger numbers of events.

Aftershock sequences or the occurrence of earthquakes during the unloading portion of the stressing cycle require the operation of a process involving a time delay, such as fracture coalescence, rupture nucleation, or fluid diffusion. Since the simple Coulomb failure model has no provision for delayed failure, it cannot, by itself, explain these phenomena. Delayed failure, even in the absence of oscillatory stress, is well known in rock mechanics as static fatigue and has been shown to result from time-dependent crack growth. Similar processes may be operative during earthquake nucleation. Our single degree of freedom numerical simulations using a rate- and displacement-dependent friction rheology were more successful than simulations based on Coulomb failure in reproducing the behavior observed in the laboratory experiments.

Appendix

Extrapolation of our laboratory observations suggests that when the tectonic loading of a fault system is modulated by a

low-amplitude periodic signal such as the Earth tides, the influence on the timing of earthquakes may be a very small signal compared to the overall uncorrelated response. In this section we show how the ability to identify weak correlations improves as $\sqrt{N}$ in a manner closely related to the improvement of signal-to-noise ratio of a repeating signal in a time series. Following the procedure outlined in section 3.2, we can express the likelihood P_{rw} that a sequence of N purely random earthquakes will wander a distance greater than D_{rw} from the origin of a phase space plot (Figure 7). Equation (3) can be modified to give

$$D_{rw} = \left(-N \ln P_{rw}\right)^{1/2}. \tag{13}$$

A coherent signal in which earthquakes tend to occur at a preferred phase angle will appear in a phase plot as a steady drift from the origin by a distance

$$\bar{D}_{cor} = \bar{v}N, \tag{14}$$

where $\bar{v}$ is the drift velocity proportional to the intensity of the correlated response. If the drift velocity is small, implying a weak correlation of earthquake timing with the forcing function, many events will be needed for a nonrandom signal to emerge. We can expect to produce a statistically significant deviation from the null hypothesis of uncorrelated earthquakes for $|D_{cor}| \approx D_{rw}$. Equating (13) and (14) gives

$$N \approx \frac{-\ln P_{rw}}{v^2}. \tag{15}$$

Equation (15) implies that if we have two processes with drift velocities v_1 and v_2 and we want to identify them at the same confidence level P_{rw}, then the relative number of earthquakes needed in the two sample populations is $N_2/N_1 = (v_1/v_2)^2$. For the case where drift velocity is proportional to the amplitude τ_m of the modulating stress function, we have $N_2/N_1 = (\tau_{m1}/\tau_{m2})^2$.

Acknowledgments. We thank J. Savage for information regarding statistical tests, moonquakes and other insights. Other helpful comments were provided by C. Scholz, J. Vidale, J. Gomberg and C. Marone. This work was supported by the National Earthquake Hazards Reduction Program.

References

Anderson, J. G., J. N. Brune, J. N. Louie, Y. Zeng, M. Savage, G. Yu, Q. Chen, and D. dePolo, Seismicity in the western Great Basin apparently triggered by the Landers, California, earthquake, 28 June 1992, *Bull. Seismol. Soc. Am., 84*, 863-891, 1994.

Blanpied, M. L., C. J. Marone, D. A. Lockner, J. D. Byerlee, and D. P. King, Quantitative measure of the variation in fault rheology due to fluid-rock interactions, *J. Geophys. Res., 103*, 9691-9712, 1998.

Cotton, L. A., Earthquake frequency, with special reference to tidal stresses in the lithosphere, *Bull. Seismol. Soc. Am., 12*, 47-198, 1922.

Dieterich, J. H., Constitutive properties of faults with simulated gouge, in *Mechanical Behavior of Crustal Rocks:The Handin Volume, Geophys. Monogr. Ser.*, vol. 24, edited by N. L. Carter et al., Washington, pp. 103-120, AGU, Washington, 1981.

Dieterich, J. H., Nucleation and triggering of earthquake slip: effect of periodic stresses, *Tectonophysics, 144*, 127-139, 1987.

Dieterich, J. H., Earthquake nucleation on faults with rate- and state-dependent strength, in *Earthquake Source Physics and Earthquake Precursors*, edited by T. Mikumo et al., pp. 115-134, Elsevier, New York 1992.

Gomberg, J., and P. Bodin, Triggering of the M_S=5.4 Little Skull Mountain, Nevada earthquake with dynamic strains, *Bull. Seismol. Soc. Am., 84*, 844-853, 1994.

Gomberg, J., and S. Davis, Stress/strain changes and triggered seismicity at The Geysers, California, *J. Geophys. Res., 101*, 733-749, 1996.

Hardebeck, J. L., J. J. Nazareth, and E. Hauksson, The static stress change triggering model: constraints from two southern California aftershock sequences, *J. Geophys. Res., 103*, 24,427-24,437, 1998.

Harris, R. A., R. W. Simpson, and P. A. Reasenberg, Influence of static stress changes on earthquake locations in southern California, *Nature, 375*, 221-224, 1995.

Hartzell, S., and T. Heaton, The fortnightly tide and the tidal triggering of earthquakes, *Bull. Seismol. Soc. Am., 79*, 1282-1286, 1989.

Heaton, T. H., Tidal triggering of earthquakes, *Bull. Seismol. Soc. Am., 72*, 2181-2200, 1982.

Hill, D. P., et al., Seismicity remotely triggered by the magnitude 7.3 Landers, California, earthquake, *Science, 260*, 1617-1623, 1993.

Holcomb, D. J., General theory of the Kaiser effect, *Int. J. Rock Mech. Min. Sci. Geomech. Abstr., 30*, 929-935, 1993.

Johnson, T., Time dependent friction of granite: implications for precursory slip on faults, *J. Geophys. Res., 86*, 6017-6028, 1981.

Kilgore, B. D., M. L. Blanpied, and J. H. Dieterich, Velocity dependent friction of granite over a wide range of conditions, *Geophys. Res. Lett., 20*, 903-906, 1993.

Kilston, S., and L. Knopoff, Lunar-solar periodicities of large earthquakes in southern California, *Nature, 304*, 21-25, 1983.

King, G. C. P., R. S. Stein, and J. Lin, Static stress changes and the triggering of earthquakes, *Bull. Seismol. Soc. Am., 84*, 935-953, 1994.

Klein, F. W., Earthquake swarms and the semidiurnal solid earth tide, *Geophys. J. R. Astron. Soc., 45*, 245-295, 1976.

Kranz, R. L., The effects of confining pressure and stress difference on static fatigue of granite, *J. Geophys. Res., 85*, 1854-1866, 1980.

Lammlein, D. R., G. V. Latham, J. Dorman, Y. Nakamura, and M. Ewing, Lunar seismicity, structure, and tectonics, *Rev. Geophys., 12*, 1-21, 1974.

Lockner, D. A., The role of acoustic emission in the study of rock fracture, *Int. J. Rock Mech. Min. Sci. Geomech. Abstr., 30*, 883-899, 1993.

Lockner, D. A., A generalized law for brittle deformation of Westerly granite, *J. Geophys. Res., 103*, 5107-5123, 1998.

Lockner, D. A., and J. D. Byerlee, An example of slip instability resulting from displacement-varying strength, *Pure Appl. Geophys., 133*, 398-410, 1990.

Melchior, P. J., *The Tides of the Planet Earth*, 458 pp., Pergamon, Tarrytown, N. Y., Oxford, 1983.

Okubo, P. G., and J. H. Dieterich, State variable fault constitutive relations for dynamic slip, in *Earthquake Source Mechanics, Geophys. Monogr. Ser.*, vol. 37, edited by S. Das, J. Boatwright, and C. H. Scholz, pp. 25-35, AGU, Washington, D. C., 1986.

Reasenberg, P. A., and R. W. Simpson, Response of regional seismicity to the static stress change produced by the Loma Prieta earthquake, *Science, 955*, 1687-1690, 1992.

Ruina, A. L., Slip instability and state variable friction laws, *J. Geophys. Res., 88*, 10,359-10,370, 1983.

Rydelek, P. A., and L. Hass, On estimating the amount of blasts in seismic catalogs with Schuster's method, *Bull., Seismol. Soc. Am., 84*, 1256-1259, 1994.

Rydelek, P. A., P. M. Davis, and R. Y. Koyanagi, Tidal triggering of earthquake swarms at Kilauea Volcano, Hawaii, *J. Geophys. Res, 93*, 4401-4411, 1988.

Rydelek, P. A., I. S. Sacks, and R. Scarpa, On tidal triggering of earthquakes at Campi Flegrei, Italy, *Geophys. J. Int., 109*, 125-137, 1992.

Schuster, A., On lunar and solar periodicities of earthquakes, *Proc. R. Soc. London, 61*, 455-465, 1897.

Simpson, R. W., and P. A. Reasenberg, Earthquake-induced static stress changes on Central California faults, in *The Loma Prieta, California Earthquake of October 17, 1989 - Tectonic Processes and Models*, edited by R. W. Simpson, U.S. Geol. Surv. Prof. Pap., 1550-F, F55-F89, 1994.

Stein, R. S., G. C. P. King, and J. Lin, Stress triggering of the 1994 M = 6.7 Northridge, California, earthquake by its predecessors, *Science, 265*, 1432-1435, 1994.

Stein, R. S., A. A. Barka, and J. D. Dieterich, Progressive failure on the North Anatolian fault since1939 by earthquake stress triggering, *Geophys. J. Int., 128*, 594-604, 1996.

Tsuruoka, H., M. Ohtake, and H. Sato, Statistical test of the tidal triggering of earthquakes: Contribution of the ocean tide loading effect, *Geophys. J. Int., 122*, 183-194, 1995.

Tullis, T. E., and J. D. Weeks, Constitutive behavior and stability of frictional sliding of granite, *Pure Appl. Geophys., 124*, 384-414, 1986.

Vidale, J., D. Agnew, C. Rodriguez, D. Oppenheimer, and H. Houston, A weak correlation between earthquakes and extensional normal stress and stress rate from lunar tides, *EOS Trans. AGU, 79, Fall Meet. Suppl.*, F640, 1998a.

Vidale, J. E., D. C. Agnew, M. J. S. Johnston, and D. H. Oppenheimer, Absence of earthquake correlation with Earth tides: an indication of high preseismic fault stress rate, *J. Geophys. Res., 103*, 24,567-24,572, 1998b.

Wiederhorn, S. M., and L. H. Bolz, Stress corrosion and static fatigue of glass, *J. Am. Ceram. Soc., 53*, 543-548, 1970.

N.M. Beeler and D.A. Lockner, Earthquake Hazards Team, U.S. Geological Survey, MS 977, 345 Middlefield Rd, Menlo Park, CA 94025. (nbeeler@isdmnl.wr.usgs.gov; dlockner@isdmnl.wr.usgs.gov.)

(Received January 12, 1999; revised May 26, 1999; accepted June 4, 1999.)